

# COMBUSTION-DERIVED $\text{La}_{1-x}\text{Sr}_x\text{Mn}_{0.5}\text{Cr}_{0.5}\text{O}_{3\pm\delta}$ ( $x = (0.20, 0.25)$ ) PEROVSKITE: PREPARATION, PROPERTIES, CHARACTERIZATION

## Z ZGOREVNO SINTEZO PRIDOBLEN PEROVSKIT $\text{La}_{1-x}\text{Sr}_x\text{Mn}_{0.5}\text{Cr}_{0.5}\text{O}_{3\pm\delta}$ ( $x = (0,20, 0,25)$ ): PRIPRAVA, LASTNOSTI, KARAKTERIZACIJE

**Klementina Zupan, Marjan Marinšek**

Faculty of Chemistry and Chemical Technology, University of Ljubljana, Aškerčeva 5, 1000 Ljubljana, Slovenia  
klementina.zupan@fkkt.uni-lj.si

*Prejem rokopisa – received: 2013-11-14; sprejem za objavo – accepted for publication: 2013-12-17*

Lanthanum-strontium-manganese-chromium-oxide-based ceramics (LSCM) are a suitable alternative to custom anode cermets in high-temperature fuel cells based on nickel and doped zirconia since they are more tolerant to sulphur poisoning. Moreover, LSCM-based anodes do not catalyse side reactions of carbon deposition during hydro-carbon fuel oxidation. A  $\text{La}_{1-x}\text{Sr}_x\text{Mn}_{0.5}\text{Cr}_{0.5}\text{O}_{3\pm\delta}$  ( $x = (0.20, 0.25)$ ) perovskite was prepared via a citrate-nitrate combustion reaction. Since any secondary phases developed during the synthesis may influence the final anode material properties, the phase development during the gel transformation was followed with a high-temperature X-ray analysis, EDS and thermal analysis. The microstructure of the LSCM elements sintered at various temperatures was studied in correlation with their electrical properties and described in accordance with the sine-wave model.

Keywords: citrate-nitrate combustion synthesis, oxide LSCM anode, phase development, sine-wave model

Keramike na osnovi lantan-stroncij-mangan-kromovega oksida (LSCM) pomenijo alternativo navadnim anodam v visokotemperaturnih gorivnih celicah, narejenih na osnovi kermetov niklja in dopiranega cirkonijevega oksida, ker niso občutljive za nečistoče v gorivu, posebej za žveplo. Prav tako anode na osnovi LSCM v mnogo manjši meri katalizirajo stransko reakcijo odlaganja ogljika pri oksidaciji goriva. Perovskitna materiala  $\text{La}_{1-x}\text{Sr}_x\text{Mn}_{0.5}\text{Cr}_{0.5}\text{O}_{3\pm\delta}$  ( $x = (0,20, 0,25)$ ) smo pripravili z zgorevanjem citratno-nitratnega gela. Ker morebitne sekundarne faze, nastale med sintezo, lahko vplivajo na lastnosti končnega produkta, smo razvoj faz pri pretvorbi gela spremljali z visokotemperaturno rentgensko analizo, EDS in termično analizo. Preučevali smo mikrostrukturo vzorcev LSCM, sintranih pri različnih temperaturah, v povezavi z njihovimi električnimi lastnostmi, kar smo opisali z modelom "sine-wave".

Ključne besede: citratno-nitratna zgovalna sinteza, oksidna LSCM-anoda, razvoj faz, model sine-wave

## 1 INTRODUCTION

Fuel cells are electrochemical reactors in which the chemical energy of the fuel is converted directly into electrical energy. They are inherently more efficient than most energy converters. In a wide group of fuel cells, the high-temperature type (SOFC) has additional advantages due to its ability to utilize high-temperature exhaust for a cogeneration of heat and its ability for internal reforming.

The cermet based on nickel and yttria-stabilized zirconia (Ni/YSZ) has been used as the anode material in high-temperature fuel cells for over 30 years.<sup>1</sup> This material exhibits a mixed electronic-ionic conductivity, favouring a fuel combustion reaction inside a porous anode. The ionic conductivity originates from the oxygen ions' transport through the oxygen-vacant sites in YSZ. Nickel-based anodes are difficult to run on dry methane and higher hydrocarbons due to undesirable carbon deposition<sup>2</sup> and their sensitivity to sulphur poisoning.<sup>3</sup> The development of the anodes in which electron transport is provided through ceramic components rather than metals has been perhaps the most

exciting area of anode research in recent years. Studies<sup>4,5</sup> have shown that complex metal oxides, such as a SrO-doped oxide-ion defective perovskite, i.e.,  $\text{La}_{1-x}\text{Sr}_x\text{Mn}_{0.5}\text{Cr}_{0.5}\text{O}_{3\pm\delta}$  (LSCM), can serve as possible replacements for Ni-based anode materials, due to a reasonable catalytic activity towards hydrogen and methane oxidation, a consistent thermal coefficient with YSZ and a good chemical stability when in contact with a standard electrolyte and interconnect materials. LSCM also exhibits a sulphur-tolerant behaviour for low  $\text{H}_2\text{S}$  concentrations in fuels and a good resistance to carbon deposition when used with hydrocarbon fuels.<sup>6</sup>

The preparation of multi-component oxides like LSCM is generally carried out with the calcining method.<sup>7</sup> Several other synthetic techniques have also been used to prepare LSCM powders, including the chelating method,<sup>8</sup> coprecipitation,<sup>9</sup> gel casting<sup>10</sup> and combustion synthesis.<sup>11-14</sup> In view of the LSCM synthesis, the solution-combustion method is especially interesting due to its ability to produce ultrafine metal-oxide powders that can be sintered at relatively low temperatures. Specifically, the electrocatalytic performances of the anode in SOFCs are critically dependent on its

microstructure (indirectly on the sintering temperature of the prepared LSCM powder, the degree of reaction conversion and phase formation).

The most commonly studied LSCM material is that with a composition of  $\text{La}_{0.75}\text{Sr}_{0.25}\text{Mn}_{0.5}\text{Cr}_{0.5}\text{O}_{3\pm\delta}$ .<sup>7</sup> There are some contradictory descriptions regarding the role of strontium in the LSCM material. Some authors claim that a higher strontium amount in LSCM increases its electrical conductivity<sup>15,16</sup>; however, according to the latest research a sufficient electrical conductivity of the LSCM material is assured even without a strontium addition.<sup>17</sup> The presence of manganese, which undergoes redox-state changes in the anode-reducing environment, results in the formation of oxygen vacancies and the development of mixed electronic/ionic conductivity.

In this work, we prepared a  $\text{La}_{1-x}\text{Sr}_x\text{Mn}_{0.5}\text{Cr}_{0.5}\text{O}_{3\pm\delta}$  ( $x = (0.20, 0.25)$ ) perovskite via a modified citrate-nitrate combustion synthesis. To describe the relationship between the conductivity of the porous material and its relative density, a novel mathematical approach was proposed:<sup>18</sup> the conductivity of highly porous materials can be expressed with a model of a rotating sine-wave function. By changing the ratio of the contribution of two sine waves, one representing the shape of each grain and the other the shape of the bottleneck between the particles, the change in electrical conductivity  $\sigma$  versus the change in material relative density  $\rho/\rho_0$  can be presented.

## 2 EXPERIMENTAL PROCEDURE

The samples with the nominal compositions of  $\text{La}_{0.75}\text{Sr}_{0.25}\text{Mn}_{0.5}\text{Cr}_{0.5}\text{O}_{3\pm\delta}$  (La0.75) and  $\text{La}_{0.80}\text{Sr}_{0.20}\text{Mn}_{0.5}\text{Cr}_{0.5}\text{O}_{3\pm\delta}$  (La0.80) were prepared using a modified citrate-nitrate combustion reaction. Stoichiometric amounts of metal nitrates  $\text{La}(\text{NO}_3)_3 \cdot 6\text{H}_2\text{O}$ ,  $\text{Sr}(\text{NO}_3)_2$ ,  $\text{Cr}(\text{NO}_3)_3 \cdot 9\text{H}_2\text{O}$  and  $\text{Mn}(\text{NO}_3)_2 \cdot 4\text{H}_2\text{O}$  and citric acid (analytical reagent grade) were dissolved with minimum quantities of water. The starting solution was prepared by mixing the five reactant solutions and then kept over a water bath at 60 °C under vacuum ( $p = 5\text{--}7$  mbar) until it transformed into a dark violet gel (at least 5 h). The initial citrate/metal and citrate/nitrate molar ratios in the starting solution were 0.53 and 0.20, respectively. The corresponding citrate-nitrate gel was then gently milled in an agate mortar and uni-axially pressed into pellets ( $\Phi = 12$  mm,  $h = 30$  mm,  $p = 17$  MPa). These samples were placed on a corundum plate and ignited at the top of the pellet with a hot tip to start a self-sustaining reaction that spreads as a reaction zone throughout the pellet. A rapid increase in the temperature inside the reaction zone was presented as a temperature profile using an optical pyrometer (Impac, IPE 140, based on the sample brightness). The measuring range of the pyrometer is from 50 to 1200 °C and it has a very quick response time (1.5 ms). The accuracy of the optically measured temperature was  $\pm 2.5$  % below 400 °C and  $\pm 0.4$  % of a measured value (in °C) above 400 °C. During the exothermic combustion

reaction, high temperatures are reached in a very short reaction time, yielding a fine-powdered product.

The thermal behaviour (TG, DTG) of the reactive gels prior to the combustion was followed with a thermogravimetric analysis (Mettler Toledo TA 3000) at a heating rate of 20 K/min. The reactive gel mass was  $\approx 5$  mg to avoid an uncontrolled self-sustaining reaction. High-temperature X-ray powder-diffraction measurement was performed on the reactive gel with a PANalytical X'Pert PRO (HTK) apparatus; a mixture 50 mg (the reaction gel and alumina in a mass ratio of 1 : 1) was gently homogenized in an agate mortar to prevent uncontrolled combustion during the analysis. Data were collected in the range of  $2\theta$  from 20° to 90° in the steps of 0.033° from room temperature to 1200 °C every 100 °C.

The synthesized powders were milled in the agate mortar and then finally wet milled in isopropanol in a planetary mill for 3 h. The as-synthesized and calcined samples (after the combustion reaction) were also analysed with the PANalytical X'Pert PRO MPD apparatus. The calcined and milled powders were subsequently uni-axially pressed into pellets (100 MPa). The formed pellets were sintered at different temperatures (1200, 1300, 1400 and 1500) °C for 1 h. For the microstructural quantitative evaluations, the sintered pellets were polished (diamond pastes of 3  $\mu\text{m}$  and 0.25  $\mu\text{m}$ ), thermally etched, and subsequently analysed with a FEG-SEM (Zeiss ULTRA plus) operated at 2 kV. The quantitative analyses of the microstructures were performed on digital images (the images were digitized into pixels with 255 different grey values) using Zeiss KS300 3.0 image-analysis software. The prepared sintered pellets were characterized with the impedance-spectroscopy technique. A polythermal quartz cell was employed to perform these tests in the temperature range from 370–910 °C in a  $\text{H}_2/\text{Ar}$  atmosphere. The impedance was measured using a Solartron 1250 analyser over the frequency range from 0.01 Hz to 65500 Hz. Prior to the impedance measurement, all the analysed tablets were sputtered with Au at both end surfaces of the discs to achieve a good electrical contact between the Pt electrodes and the measured samples.

## 3 RESULTS AND DISCUSSION

One of the major advantages of a combustion synthesis is a rapid temperature change during the reaction (both during heating due to the combustion reaction or cooling after the reaction). Consequently, due to a relatively short time of the exposure of the system to the temperatures at which diffusion plays an important role in the system rearrangement, the as-synthesized product remains as an ultrafine powder with nanoscaled grains. Since a self-sustaining combustion is characterized by big temperature gradients around the reaction zone, typical temperature profiles of the chosen citrate-nitrate systems are presented in **Figure 1**. The peak temperatu-

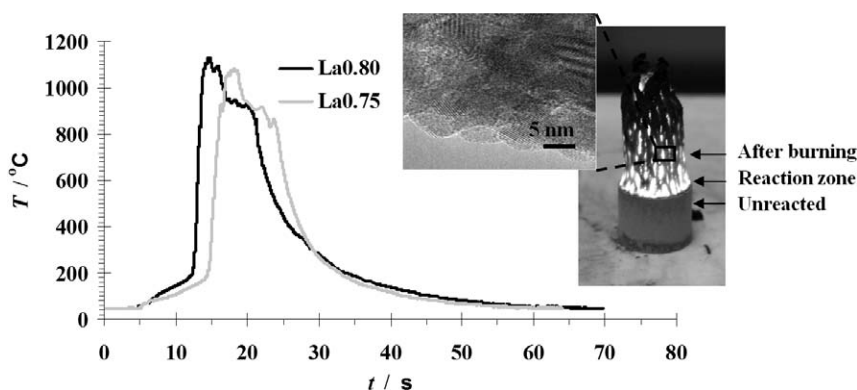


**Figure 1:** Typical temperature profiles measured in a single spot (for La0.75 and La0.80 samples) together with a photograph of the citrate-nitrate-gel combustion process for the LSCM preparation

**Slika 1:** Značilen temperaturni profil, merjen v eni točki (za vzorca La0,75 in La0,80) skupaj s fotografijo zgorovalne sinteze citratno-nitratnega gela

res reached during the synthesis are 1080 °C and 1130 °C for samples La0.75 and La0.8, respectively. The reaction-zone propagation-wave velocity is around 0.6 mm s<sup>-1</sup>, while the maximum temperature gradient at the head of the reaction zone is 592 °C s<sup>-1</sup> and 679 °C s<sup>-1</sup> for La0.75 and La0.8, respectively. The samples cooled down from their peak temperatures to 50 °C in approximately 45 s (and from the peak temperatures to 500 °C in ≈ 10 s).

The citrate-nitrate combustion of the reaction gel results in the formation of mixed oxide and the elimination of some volatile products, i.e., CO<sub>2</sub>, CO, H<sub>2</sub>O, NO and N<sub>2</sub>.<sup>19</sup> The mass changes during the combustion were measured with a TG-DTG analysis and are presented in **Figure 2**. The citrate-nitrate gel decomposes into the final LSCM product in several consecutive steps. The first temperature range of the mass loss occurred between 25 °C and 100 °C, due to the moisture evaporation. This step is followed by three more pronounced steps in the temperature intervals from 100 °C to 190 °C, from 190 °C to 300 °C and from 300 °C to 400 °C, respectively, that were attributed to the citrate-nitrate combustion itself.<sup>19</sup> According to the classification proposed by Courty et al.,<sup>20</sup> the citrate-nitrate combustion that takes place in several consecutive stages corresponds to the Type II combustion reaction, while the Type I reaction occurs in the continuous and vigorous mode if the reaction mixture contains catalytically active metal ions, i.e., Fe, Ni, Ag, Cu or Co. The citrate-nitrate combustion is completed at 400 °C. The final two minor mass changes observed at the temperatures around 580 °C and 710 °C, respectively, are probably associated with some secondary phase reaction and a complete oxidation of residual carbon. Residual carbon is a common consequence when the combustion is conducted in a non-oxidative surrounding atmosphere. The non-oxidative surrounding atmosphere originates from the citrate-nitrate combustion reaction, which produces relatively large amounts of the previously mentioned volatile products.

As predicted from the thermal behaviour of the reactive gel, the phase development in the precursor is related to the mass changes at different stages during the thermal treatment. The sequence of the crystalline phases formed during the heating of the La0.75 gel is followed by a high-temperature XRD analysis (**Figure 3**). Prior to the analysis, the gel was diluted with corundum to prevent premature ignition of the reaction mixture and uncontrolled propagation of the combustion reaction. It is apparent that the reactive gel prior to the combustion and the early intermediate products up to 500 °C are mostly amorphous (the diffraction peaks marked with **A** belong to the diluting agent Al<sub>2</sub>O<sub>3</sub>). Beside the amorphous phase, the reactive gel also contains a small amount of a cubic modification of Sr(NO<sub>3</sub>)<sub>2</sub>. The appearance of Sr(NO<sub>3</sub>)<sub>2</sub> in the starting reactive gel is somewhat unexpected because slightly fuel-rich conditions are adjusted in the reactive gel with a view to eliminating the strontium nitrate. However, Baythoun and Sale<sup>21</sup> also reported that Sr(NO<sub>3</sub>)<sub>2</sub> appeared in the citrate precursor. In the temperature range up to 500 °C, strontium nitrate transforms into strontium nitrite oxide (SrN<sub>2</sub>O<sub>2</sub>). Simultaneously, carbon appears in the system as a consequence of incomplete citrate combustion. In the reactive gel heated up to 600 °C, the small amount of carbon is the only crystalline phase in the system. The precursor transforms into a LSCM perovskite in the temperature interval between 600 °C and 700 °C. The observed LSCM formation is in agreement with the TG measurements, in which the final mass changes in the system are observed at ≈ 580 °C and ≈ 710 °C. These mass losses may be correlated with the decomposition of strontium nitrite oxide into strontium oxide and the residual-carbon burning, respectively.

Since the citrate-nitrate combustion reaches the temperatures well above 1000 °C, LSCM is expectedly the main crystalline phase in the as-prepared sample. However, due to the rapid temperature change in the reaction zone, some secondary phases may also appear in the product. According to the XRD patterns, in the as-prepared

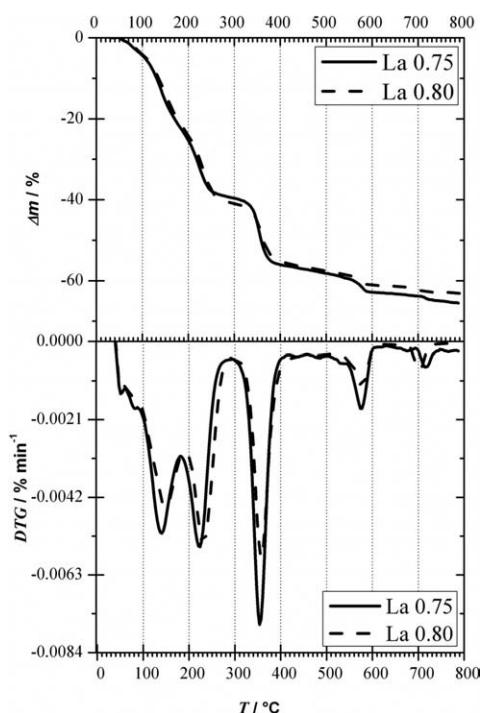


**Figure 2:** Mass change of La0.75 and La0.80 citrate-nitrate gels taken in air atmosphere followed by TG-DTG analysis

**Slika 2:** Sprememba mase citratno-nitratnih gelov vzorcev La0,75 in La0,80 v zraku, posneta z analizo TG-DTG

sample and in the sample subsequently calcined at 400 °C, a polytypic, Ruddlesden-Popper type compound  $\text{Sr}_2\text{CrO}_4$  is formed. This strontium-rich phase is expected to form during the synthesis in an oxygen-deficient atmosphere.<sup>22</sup> The calcination at 800 °C triggers a reaction of  $\text{Sr}_2\text{CrO}_4$  with the oxygen from the surrounding

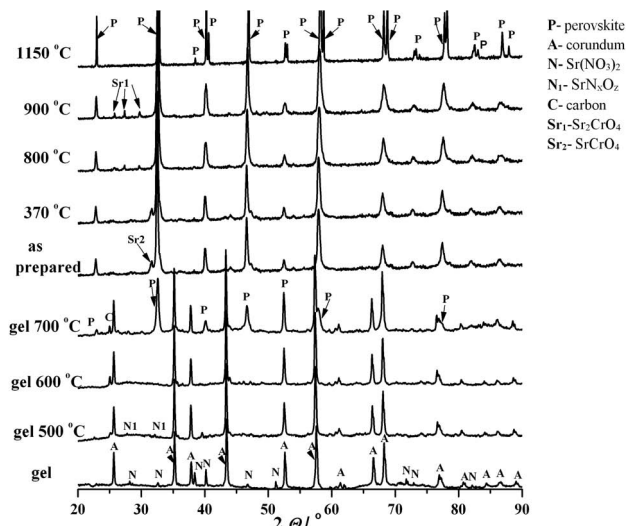


**Figure 3:** Crystalline-phase development during the stepwise thermal treatment of La0.75 precursor and observed crystalline phases in the as-synthesized and calcined products

**Slika 3:** Razvoj kristalnih faz v La0,75-prekursorju med postopnim segrevanjem in fazna sestava po sintezi ter kalcinaciji pri različnih temperaturah

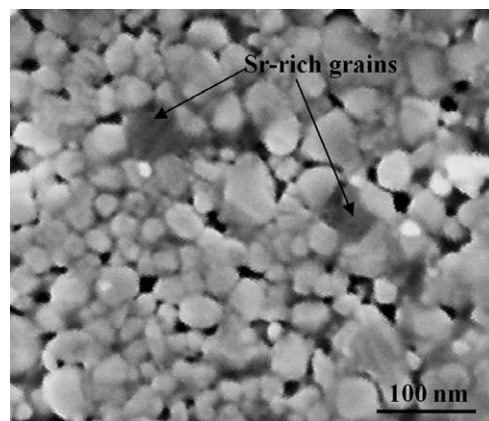


**Figure 4:** SEM micrograph of sample La0.75 after the calcination at 900 °C

**Slika 4:** SEM-slika vzorca La0,75 po kalcinaciji pri 900 °C

atmosphere, forming  $\text{SrCrO}_4$ , which also remains in the system at 900 °C. After the calcination at 1150 °C, the only phase present in the product is the LSCM perovskite.

XRD diffractograms of samples La0.75 and La0.80 show that their phase developments are practically identical.

A scanning electron micrograph of sample La0.75 calcined at 900 °C is shown in **Figure 4**. The sample is composed of spherical particles under 100 nm in size, bound into agglomerates. Between the main LSCM grains, in several spots, a strontium-rich phase is observed as dark grey grains. The SEM analysis confirms the presence of a  $\text{SrCrO}_4$  secondary phase and it is consistent with the X-ray diffraction pattern of the sample after the calcination at 900 °C.

As mentioned in the introduction, the sintering behaviour of the LSCM ceramics is very important for its application in the SOFC technology. One of the major problems in using LSCM as an anode material is its relatively high sintering temperature. For this reason, creating good contacts between LSCM particles at the lowest possible sintering temperature makes the material more attractive and raises its potential applicability for making a multilayer SOFC membrane. Furthermore, good contacts between the particles are essential in creating continuous paths through a sintered element, consequently reaching a high conductivity.

The sintering behaviours of both synthesized LSCM materials (La0.75 and La0.80) are demonstrated in **Figure 5**. Since all the parameters important for an exact analysis are sometimes difficult to simply obtain from SEM micrographs, an in-depth quantitative microstructural analysis was performed on the sintered samples. For statistically reliable data at each chosen temperature, five to ten different regions on the surfaces of the tablets were analysed. The results of the quantitative microstructural analysis are summarized in **Table 1**. Parameters  $\rho_{rel.}$ ,  $\epsilon$ ,  $\bar{d}$  and  $\Psi$  represent the relative sintered

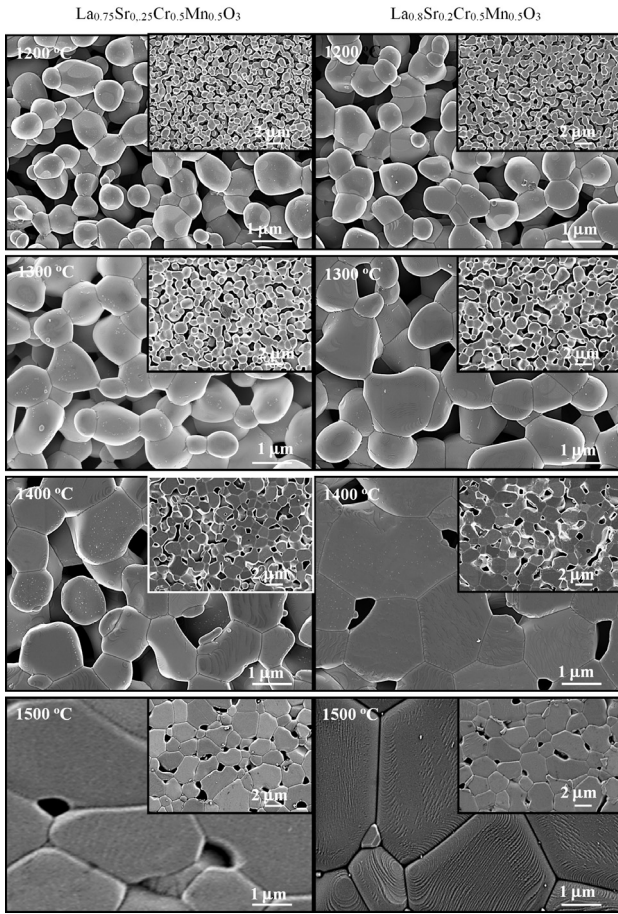


**Figure 5:** SEM micrographs of LSCM ceramics sintered at various temperatures (left column for  $\text{La}_{0.75}$  and right column for  $\text{La}_{0.80}$ )  
**Slika 5:** SEM-posnetki LSCM-keramike, sintrane pri različnih temperaturah (levi stolpec  $\text{La}_{0.75}$  in desni stolpec  $\text{La}_{0.80}$ )

density, the geometrical porosity of sintered pellets, the diameter of the area-analogue circle DCIRCLE and the shape factor expressed as FCIRCLE, respectively. According to the results of the quantitative microstructural analysis, the relative sintered density expectedly increases and, on the contrary, the porosity decreases with the increasing sintering temperature.  $\text{La}_{0.80}$  sinters to somewhat higher densities than  $\text{La}_{0.75}$ . At the highest sintering temperature (1500 °C)  $\rho_{\text{rel.}}$  reaches 90.21 % and 94.46 % for  $\text{La}_{0.75}$  and  $\text{La}_{0.80}$ , respectively. The higher sintering temperature also results in a pronounced grain growth so that at 1500 °C the original sub-micrometre grains grow up to almost  $\approx 2 \mu\text{m}$ . An interesting phenomenon is observed regarding the shape factor: with the

pronounced growth, the grains become more irregular, which is manifested with a slight decrease in their shape factor. However, one very important finding arises from the microstructural analysis. By increasing the sintering temperature, the contact areas between the grains are enlarged, making it progressively easier to find solid continuous paths through the samples.

The calculated specific electrical conductivity of the sintered LSCM ceramics is shown in **Figure 6**. Both samples exhibit the expected  $\sigma$  vs.  $T$  relationship, in which  $\sigma$  increases with the increasing  $T$ . It is also evident from **Figure 6** that  $\sigma$  depends on the material's micro-

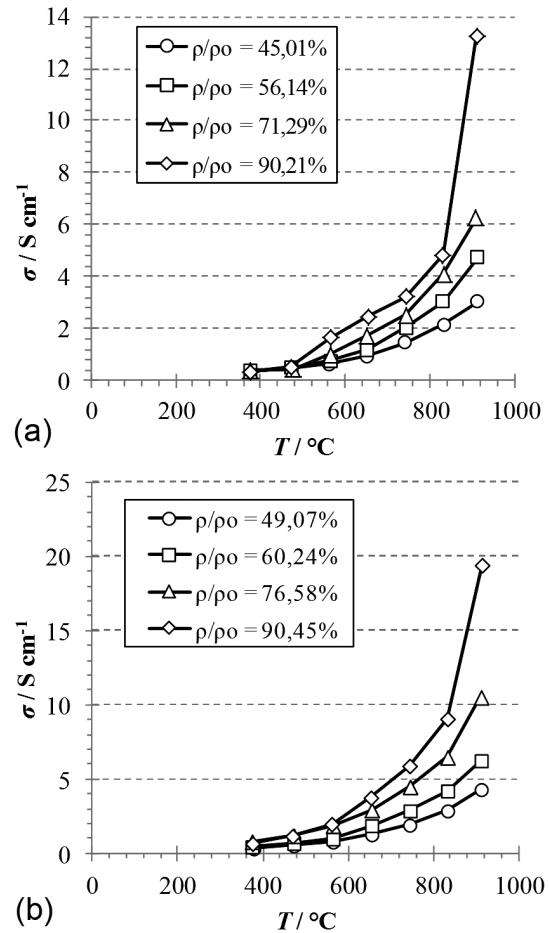


**Figure 6:** Relationship  $\sigma$  vs.  $T$  for LSCM ceramics sintered at various temperatures: a)  $\text{La}_{0.75}$  and b)  $\text{La}_{0.80}$

**Slika 6:** Specifična električna prevodnost ( $\sigma$ ) v odvisnosti od temperature ( $T$ ), merjeno pri različnih temperaturah: a)  $\text{La}_{0.75}$  in b)  $\text{La}_{0.80}$

**Table 1:** Quantitative microstructural analysis of  $\text{La}_{0.75}\text{Sr}_{0.25}\text{Cr}_{0.5}\text{Mn}_{0.5}\text{O}_3$  and  $\text{La}_{0.8}\text{Sr}_{0.2}\text{Cr}_{0.5}\text{Mn}_{0.5}\text{O}_3$  ceramics

**Tabela 1:** Kvantitativna analiza mikrostrukture keramike  $\text{La}_{0.75}\text{Sr}_{0.25}\text{Cr}_{0.5}\text{Mn}_{0.5}\text{O}_3$  in  $\text{La}_{0.8}\text{Sr}_{0.2}\text{Cr}_{0.5}\text{Mn}_{0.5}\text{O}_3$

$T_s / ^\circ\text{C}$	$\text{La}_{0.75}$				$\text{La}_{0.80}$			
	$\rho_{\text{rel.s.}} / \%$	$\epsilon / \%$	$\bar{d} / \mu\text{m}$	$\Psi$	$\rho_{\text{rel.s.}} / \%$	$\epsilon / \%$	$\bar{d} / \mu\text{m}$	$\Psi$
1200	45.01	54.99	0.47	0.86	49.07	50.93	0.50	0.85
1300	56.14	43.86	0.80	0.84	60.25	39.76	0.89	0.85
1400	71.29	28.71	1.11	0.81	76.58	23.42	1.38	0.81
1500	90.21	9.79	1.67	0.79	94.46	5.54	1.91	0.83

structure. At a chosen measuring temperature, the samples sintered to a higher relative density show a rather high specific electrical conductivity. By comparing the absolute  $\sigma$  values of both samples, La0.80 exhibits higher  $\sigma$  values. These higher  $\sigma$  values and the material densification at lower temperatures make the La0.80 sample superior to the La0.75 sample. Such a finding may be, at first glance, a bit surprising as higher Sr amounts in LSCM ceramics should result in a superb electrical conductivity.<sup>15,16</sup> However, the La0.75 sample also contains higher concentrations of secondary phases, such as  $\text{SrCrO}_4$ . Secondary phases are always low conductive phases, precipitating at the grain boundaries of the primary LSCM phase. As a result, any amount of a secondary phase, sometimes not even detectable with the XRD analysis, lowers the overall electrical conductivity of a sample.

The apparent conductivity of the sintered LSCM samples is sensitive to their relative density or porosity. For this reason, the  $\sigma/\sigma_0$  vs.  $\rho/\rho_0$  (or  $\varepsilon$ ) relationship of La0.75 and La0.80 is demonstrated in **Figure 6** ( $\rho_0$  and  $\sigma_0$  values denote the theoretical density and specific electrical conductivity of a fully dense material, respectively). Since fully dense LSCM ceramics are rather difficult to prepare, the  $\sigma_0$  values were estimated by creating a  $\sigma$  vs.  $\rho$  relationship. This relationship shows a linear dependence from which  $\sigma_0$  at calculated  $\rho_0$  can be estimated. The estimated  $\sigma_0$  values of La0.75 and La0.80 are 14.35 S/cm and 21.10 S/cm, respectively.

The observed results of the relative conductivity vs. relative density dependence for the two LSCM samples are essentially consistent with the sine-wave approximation of the conductivity change for porous materials. The scattering of the observed results around the theoretically predicted curves may be attributed to the inaccuracy of the conductivity measurements or some microstructural defects of the measured bodies, such as micro-cracks, low-scale material inhomogeneity, inhomogeneous grain size and shape or local packing disorder. According to the results presented in **Figure 7**, the LSCM-relative conductivity reaches rather low values as the sintering temperature does not exceed 1200 °C. Such a result is a consequence of a relatively low temperature for the LSCM sintering. The densification process of LSCM starts at  $\approx 1100$  °C. Below 1100 °C, the prepared LSCM tablets are in a green state with the typical relative density of green bodies, i.e., 40–50 %. In the green state LSCM particles remain isolated except for the point contacts between them, meaning that the observed overall conductivity is negligible. With the rising sintering temperature, the temperature-dependent sintered densities increase, ensuring better contacts between the particles that are demonstrated through higher relative conductivities. From this perspective, the sintering temperature plays an essential role when LSCM ceramics are used for an anode preparation in SOFC. During a multilayer-membrane preparation, where the

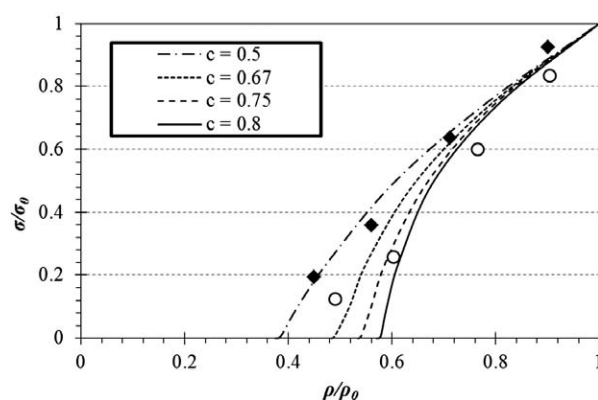


**Figure 7:** Calculated relationships between relative density  $\rho/\rho_0$  or porosity  $\varepsilon$  and relative conductivity  $\sigma/\sigma_0$  for different microstructural parameters  $c$ ; (solid, dashed and dotted lines used as described by Mizusaki et al.<sup>11</sup>) and the observed trend of the measured data ( $\blacklozenge$  La0.75 and  $\circ$  La0.80)

**Slika 7:** Izračunana zveza med relativno gostoto  $\rho/\rho_0$  ali poroznostjo  $\varepsilon$  in relativno prevodnostjo  $\sigma/\sigma_0$  za različne mikrostrukturne parametre  $c$ ; (polna, prekinjena in pikčasta črta, kot je to opisal Mizusaki et al.<sup>11</sup>) in usmeritev merjenih podatkov ( $\blacklozenge$  La0,75 in  $\circ$  La0,80)

anode, electrolyte and cathode materials are co-sintered, the sintering temperatures (of course, for a desired microstructure) are preferable to be as low as possible. With a relatively low sintering temperature, any potential interlayer reaction is less likely to occur. Among the investigated LSCM compositions, the La0.80 not only exhibits a higher electrical conductivity but, relative to La0.75, also sinters at somewhat lower temperatures, ensuring broader contacts between individual particles at any given preparation temperature. These findings clearly favourite La0.80 over La0.75 and make the LSCM compositions with a slightly higher La : Sr molar ratio more appropriate for the SOFC anode-material preparation.

## 4 CONCLUSIONS

Ultrafine LSCM products with various amounts of strontium,  $\text{La}_{1-x}\text{Sr}_x\text{Mn}_{0.5}\text{Cr}_{0.5}\text{O}_{3\pm\delta}$  ( $x = (0.20, 0.25)$ ), were prepared via a citrate-nitrate combustion synthesis. A rapid temperature change during the combustion reaction (several hundreds of °C  $\text{s}^{-1}$ ) and a relatively short time of the exposure of the system to the temperatures at which the final grains can grow keep the prepared LSCM particles in the nanometer scale.

The TG/DTG analysis indicates that the citrate-nitrate gel decomposes into the final LSCM product in several consecutive steps, starting with the moisture evaporation (up to  $\approx 110$  °C), the citrate-nitrate combustion reaction (up to 400 °C) and ending with the secondary-phase reaction (at  $\approx 580$  °C) and the residual-carbon elimination (at  $\approx 710$  °C). The reactive gel prior to the combustion and the early intermediate products heated up to 500 °C are mostly amorphous, containing a small amount of  $\text{Sr}(\text{NO}_3)_2$ , which with a prolonged time or increased temperature transforms into

strontium nitrite oxide ( $\text{SrN}_2\text{O}_z$ ). At the same stage, residual carbon appears in the system as a consequence of incomplete citrate combustion. The precursor transforms into a LSCM perovskite in the temperature interval between 600 °C and 700 °C, which is in agreement with the TG measurements, during which the final mass changes in the system are observed.

The relative sintered density of the prepared LSCM tablets expectedly increases with the increasing sintering temperature, while the contact area between the grains is enlarged, making it progressively easier to find a solid continuous path throughout the samples. Sample La0.80 sinters to somewhat higher densities than La0.75. The highest sintering temperature (1500 °C) results in the relative densities of 90.21 % and 94.46 % for La0.75 and La0.80, respectively.

When comparing the absolute  $\sigma$  values of both samples, La0.80 exhibits higher  $\sigma$  values. Specifically, higher Sr contents in LSCM ceramics should result in superb electrical conductivity. However, the La0.75 sample also contains a higher concentration of the  $\text{SrCrO}_4$  secondary phase, which is a low conductive phase. The observed results for the relative conductivity vs. relative density dependence for the two LSCM samples are essentially consistent with the sine-wave approximation of the conductivity change for porous materials. Regarding the sintering temperatures and  $\sigma$  vs.  $T$  measurements, the LSCM material with the slightly higher La : Sr molar ratio is more appropriate for SOFC applications.

## 5 REFERENCES

- A. Atkinson, S. Barnett, R. J. Gorte, J. T. D. Irvine, A. J. McEvoy, M. Mogensen, S. C. Singhal, J. Vohs, Advanced anodes for high temperature fuel cells, *Nat. Materials*, 3 (2004), 17–24
- S. Macintosh, R. J. Gorte, Direct hydrocarbon solid oxide fuel cells, *Chem. Rev.*, 104 (2004), 4845–4865
- H. Hurokawa, T. Z. Shoklaper, C. P. Jacobson, L. C. De Jonghe, S. J. Visco, Ceria nanocoating for sulphur tolerant Ni-based anodes of solid oxide fuel cells, *Electrochem. Solid State*, 100 (2007), 135–138
- S. Tao, J. T. S. Irvine, Discovery and Characterisation of Novel Oxide Anodes for Solid Oxide Fuel Cells, *Chem. Rec.*, 4 (2004), 83–95
- S. P. Jiang, X. J. Chen, S. H. Chan, J. T. Kwok, GDC-Impregnated ( $\text{La}_{0.75}\text{Sr}_{0.25}$ ) ( $\text{Cr}_{0.5}\text{Mn}_{0.5}$ ) $\text{O}_3$  Anodes for Direct Utilization of Methane in Solid Oxide Fuel Cells, *J. Electrochem. Soc.*, 153 (2006), A850–A856
- S. Tao, J. T. S. Irvine, A redox-stable efficient anode for solid-oxide fuel cells, *Nat. Mater.*, 2 (2003), 320–322
- S. Tao, J. T. S. Irvine, Synthesis and characterization of ( $\text{La}_{0.75}\text{Sr}_{0.25}$ ) $\text{Cr}_{0.5}\text{Mn}_{0.5}\text{O}_{3-\delta}$ , a redox-stable, efficient perovskite anode for SOFCs batteries, fuel cells, and energy conversion, *J. Electrochem. Soc.*, 151 (2004), A252–A259
- J. Wan, J. H. Zhu, J. B. Goodenough,  $\text{La}_{0.75}\text{Sr}_{0.25}\text{Cr}_{0.5}\text{Mn}_{0.5}\text{O}_{3-\delta}$  + Cu composite anode running on  $\text{H}_2$  and  $\text{CH}_4$  fuels, *Solid State Ionics*, 177 (2006), 1211–1217
- S. B. Ha, P. S. Cho, Y. C. Cho, D. Lee, J. H. Lee, Preparation of  $\text{La}_{0.75}\text{Sr}_{0.25}\text{Cr}_{0.5}\text{Mn}_{0.5}\text{O}_{3-\delta}$  fine powders by carbonate coprecipitation for oxide fuel cells, *J. Power Sources*, 195 (2010), 124–129
- S. P. Jiang, L. Zhang, Y. Zhang, Lanthanum strontium manganese chromite cathode and anode synthesized by gel-casting for solid oxide fuel cells, *J. Mater. Chem.*, 17 (2007), 2627–2635
- M. A. Raza, I. Z. Rahman, S. Beloshapkin, Synthesis of nanoparticles of  $\text{La}_{0.75}\text{Sr}_{0.25}\text{Cr}_{0.5}\text{Mn}_{0.5}\text{O}_{3-\delta}$  (LSCM) perovskite by solution combustion method for solid oxide fuel application, *Journal of Alloys and Compounds*, 485 (2009), 593–597
- S. Zha, P. Tsang, Z. Cheng, M. Liu, Electrical properties and sulfur tolerance of  $\text{La}_{0.75}\text{Sr}_{0.25}\text{Cr}_{1-x}\text{Mn}_x\text{O}_3$  under anodic conditions, *J. Solid State Chem.*, 178 (2005), 1844–1850
- D. M. Bastidas, S. Tao, J. T. S. Irvine, A symmetrical solid oxide fuel cell demonstrating redox stable perovskite electrodes, *J. Mater. Chem.*, 16 (2006), 1603–1605
- B. Huang, S. R. Wang, R. Z. Liu, X. F. Ye, H. W. Nie, X. F. Sun, T. L. Wen, Performance of  $\text{La}_{0.75}\text{Sr}_{0.25}\text{Cr}_{0.5}\text{Mn}_{0.5}\text{O}_{3-\delta}$  perovskite-structure anode material at lanthanum gallate electrolyte for IT-SOFC running on ethanol fuel, *J. Power Sources*, 167 (2007), 39–46
- C. Lu, W. L. Worrell, R. J. Gorte, J. M. Vohs, SOFCs for Direct Oxidation of Hydrocarbon Fuels with Samaria-Doped Ceria Electrolyte Batteries and energy conversion, *J. Electrochem. Soc.*, 150 (2003), A354–A358
- X. J. Chen, Q. L. Liu, K. A. Khor, S. H. Chan, High-performance ( $\text{La,Sr}$ )( $\text{Cr,Mn}$ ) $\text{O}_3$ /( $\text{Gd,Ce}$ ) $\text{O}_{2-\delta}$  composite anode for direct oxidation of methane, *J. Power Sources*, 165 (2007), 34–40
- L. Deleebeeck, J. L. Fournier, V. Birss, Comparison of Sr-doped and Sr-free  $\text{La}_{1-x}\text{Sr}_x\text{Mn}_{0.5}\text{Cr}_{0.5}\text{O}_{3\pm\delta}$  SOFC Anodes, *Solid State Ionics*, 181 (2010), 1229–1237
- J. Mizusaki, S. Tsuchiya, K. Waragi, H. Tagawa, Y. Arai, Y. Kuwayama, Simple Mathematical Model for the Electrical Conductivity of Highly Porous Ceramics, *J. Am. Ceram. Soc.*, 79 (1996), 109–113
- K. Zupan, M. Marinšek, B. Novosel, Combustible precursor behaviour in the lanthanum chromite formation process, *Mater. Tehnol.*, 45 (2011) 5, 439–445
- P. Courty, H. Ajot, Ch. Marcilly, B. Delmon, Oxydes Mixtes ou en Solution Solide sous Forme Très Divisée Obtenus par Décomposition Thermique de Précurseurs Amorphes, *Powder Technology*, 7 (1973), 21–38
- M. S. G. Baythoun, F. R. Sale, Production of Strontium-substituted lanthanum manganite perovskite powder by the amorphous citrate process, *J. Mater. Sci.*, 17 (1982), 2757–69
- H. Yokohawa, N. Sakai, T. Kawada, M. Dokiya, Chemical Thermodynamic Considerations in Sintering of  $\text{LaCrO}_3$ -Based Perovskites, *J. Electrochem. Soc.*, 138 (1991), 1018–1027